NASA Technical Memorandum 106709
ICOMP–94–19

Progress in Grid Generation: From Chimera to DRAGON Grids

Meng-Sing Liou
Lewis Research Center
Cleveland, Ohio

and

Kai-Hsiung Kao
Institute for Computational Mechanics in Propulsion
Lewis Research Center
Cleveland, Ohio

August 1994

National Aeronautics and
Space Administration

Progress in Grid Generation: From Chimera to DRAGON Grids

Meng-Sing Liou
National Aeronautics and Space Administration
Lewis Research Center
Cleveland, Ohio 44135

Kai-Hsiung Kao
Institute for Computational Mechanics in Propulsion
National Aeronautics and Space Administration
Lewis Research Center
Cleveland, Ohio 44135

ABSTRACT

Hybrid grids, composed of structured and unstructured grids, combines best features of both. The chimera method is a major stepstone toward a hybrid grid from which the present approach is evolved. The chimera grid composes a set of overlapped structured grids which are independently generated and body-fitted, yielding a high quality grid readily accessible for efficient solution schemes. The chimera method has been shown to be efficient to generate a grid about complex geometries and has been demonstrated to deliver accurate aerodynamic prediction of complex flows. While its geometrical flexibility is attractive, interpolation of data in the overlapped regions—which in today's practice in 3D is done in a nonconservative fashion, is not. In the present paper we propose a hybrid grid scheme that maximizes the advantages of the chimera scheme and adapts the strengths of the unstructured grid while at the same time keeps its weaknesses minimal. Like the chimera method, we first divide up the physical domain by a set of structured body-fitted grids which are separately generated and overlaid throughout a complex configuration. To eliminate any pure data manipulation which does not necessarily follow governing equations, we use non-structured grids only to directly replace the region of the arbitrarilly overlapped grids. This new adaptation to the chimera thinking is coined the DRAGON grid. The nonstructured grid region sandwiched between the structured grids is limited in size, resulting in only a small increase in memory and computational effort. The DRAGON method has three important advantages: (1) preserving strengths of the chimera grid, (2) eliminating difficulties sometimes encountered in the chimera scheme, such as the orphan points and bad quality of interpolation stencils, and (3) making

grid communication in a fully conservative and consistent manner insofar as the governing equations are concerned.

To demonstrate its use, the governing equations are discretized using the newly proposed flux scheme, AUSM$^+$, which will be briefly described herein. Numerical tests on representative 2D inviscid flows are given for demonstration. Finally, extension to 3D is underway, only paced by the availability of 3D unstructured grid generator.

1 INTRODUCTION

We argue that an effective practical CFD method must pass certain criteria such as: (1) fast turnaround, and (2) accurate and reliable solution for routine calculations of engineering problems, which in general involve complex geometry. The first point entails a short setup time for calculation, minimal memory requirement, and efficient and robust solution algorithm. The second point requires a judicious choice of discretization procedure. Choice of grids will greatly influence whether the above two criteria are met satisfactorily. Recent progress toward generating grids about a complex geometry, supporting the above criteria, is the subject of this paper.

During the last decade both structured and unstructured grid techniques have been developed and applied to solution of various CFD problems. To deal with situations in which complex geometry imposes great constraints and difficulties in generating grids, composite structured grid schemes and unstructured grid schemes currently are the two mainstream approaches.

The chimera grid scheme[BSDB86, SB87, BCM$^+$89], like similar methods[Att81, CH90, BCH89], uses overset grids to resolve complex geometries or flow features and is generally classed into the composite structured grid catagory. In [Ste90], Steger further elaborates the versatility of the chimera method and indicates areas for refinement. To set a proper perspective and allow comparison with the unstructured grid method, we summarize first the strengths and weaknesses of the chimera method.

1. It is an easy, versatile, and most general way of generating structured grids about a complex geometry. Techniques for generating structured grids are mature and robust; several highly developed grid packages are available.
2. Each individual grid is of high quality—body-fitted and mostly orthogonal, which is a very desirable feature for accurate and efficient viscous calculations.
3. It allows efficient solution algorithms for both steady and unsteady calculations.
4. It is a proven and relatively mature technique for solving flows over complex configurations[SB87, BCM$^+$89] and even those in motion[MS89].
5. Solution adaptation procedures[KLC94] can be applied by simply setting grids over regions with interesting flow characteristics.

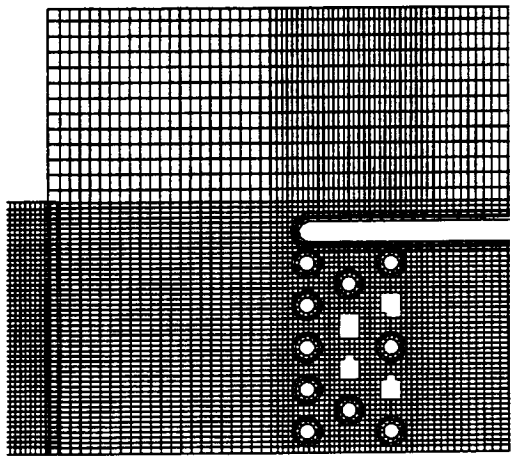

Figure 1 Chimera grid used for flow in a turbine coolant passage in which pins are placed to promote mixing. Circular grids attached to the pin are overset on the background rectangular grid on which holes (whose precise meaning is given later in §4.3) are created. Pins and their grid can be deleted and added easily to aid design analysis.

6. It is just as easy to add/delete components to/from the configuration. This flexibility clearly has great potential for design purposes. Figure 1 shows rows of pins placed in a turbine coolant passage to promote mixing. Once a circular grid is generated for a pin, a duplication of it can be added and moved to anyplace to assess the effect on performance.
7. Problems can arise in the current practice for interpolating data in the overlapped region of grids, leading to spurious and even incorrect solutions.

On the other hand, the unstructured grid method has the following strengths and weaknessess.

1. It is very flexible to generate an unstructured grid around a complex body, e.g., [JBW86, BS93, Pro93].
2. The solution adaptivity is perhaps its biggest strength[Löh87, PVMZ87].
3. It has been shown to be extremely memory and computation intensive[Gha94].
4. It is not suitable to resolve regions with a dominant direction gradient such as viscous layers near the body insofar as accuracy and efficiency are considered[HC89, SIR94].
5. Choices of efficient flow solvers are limited, thus further affecting efficiency of the method.

From the above comparison, we conclude that both methods complement each

other on strengths and weaknesses and any pure-strain approach may not achieve the criteria set forth in the beginning. Hence, a method that properly employs a hybrid of structured and unstructured grids may prove to be fruitful. In fact some hybrid schemes have already appeared[NO87, Wea88, HC89, SIR94] and have shown promising features. Interestingly enough, researchers from each camp have infused ideas from the other to appraoch a hybrid grid: a sturtured grid is embedded underneath an otherwise unstructured grid in order to better resolve the viscous region[HC89, SIR94], or an unstructured grid is used to enhance structured grid's flexibility for handling complex geometries[NO87, Wea88]. Nevertheless, there is an important difference between the above two approaches toward hybrid grids. On the one hand, a majority of region is filled with unstructured meshes, while on the other the region is mostly structured. Hence, the latter has more efficent flow solvers and more storage space at disposal, thereby resulting in fast turnaround.

Closer examination of the chimera method reveals that item 7 is the only serious problem challenging current practice—the nonconservative interpolation of data belonging to different grids. Our experiences have indicated that the interpolation error can become globally significant if numerical fluxes are not fully conserved, in particular when a discontinuity runs through the interpolated region. Also this error can be strongly affected by the underlying flux schemes, such as central vs. upwind schemes. We point out, however, that this difficulty is not inherent to the chimera method itself. It must be noted that conservative interpolation schemes in 2D[ML89, WY94] have been shown to be relatively easy. Extension to 3D in determining the volume weights for irregular polyhedra however is not all that straightforward. Even if 3D conservative interpolation proves to be feasible, a fundamental difficulty exists because how the fine-grid data is distributed to coarse grid is nonunique.

An alternative way to ensure interface conservation and avoid uncertainty on interpolation scheme altogether would be to introduce an unstructured flow solver in the vicinity of the interface boundaries, as proposed in[NO87, Wea88]. In this paper a different approach is presented which uses non-structured mesh to replace the overset region in the chimera embedded grids. We believe that this approach not only eliminates the shortcoming of the current chimera method but also preseves its advantages. The extension of the present method to three dimensions is straightforward and only paced by the capability of 3D unstructured grid generation techniques.

We will begin with the premise that the chimera grid is a formidable choice for dealing with a multi-component, complex geometry. It is difficult to argue against this method because, aside from many desirable features discussed above, it has a convincing list of successful Navier-Stokes solutions of very complex problems. This choice leaves us a clear task to tackle for our research: preserve/maximize desirable features of the method and eliminate shortcomings associated with the

current practice. This is the path and objective taken in the present paper.

2 CHIMERA GRID

Since the chimera method is a major stepstone in our development, including it in our presentation is necessary and it is useful to familiarize the reader with the chimera method. We will only highlight key elements used in the method, the interested reader should consult the literature on the subject and the interesting thoughts pondered in [Ste90].

The chimera and other like methods have two principal elements: (1) decomposition of a chosen computation domain into subdomains, and (2) communications of solution data among these subdomains. Software is needed to automatically interconnect grids of subdomains, define the holed region, and supply pointers to facilitate communication among grids during the solution process. Two major codes, namely PEGSUS[BSDB86, ST91] and CMPGRD[CH90, BCH89], using different algorithms have been developed. We have used the PEGSUS codes[BSDB86, ST91] to perform the above task. CMPGRD is also a general 3D software and has an interactive capability for 2D grids. Hereafter, we will specifically discuss the chimera grid within the capability of the PEGSUS codes. PEGSUS 4.0[ST91] is the latest release and executes four basic tasks: (1) process the grids and user inputs for all subdomains, (2) identify the hole and interpolation boundary points, (3) determine the interpolation stencil and interpolation coefficients for each interpolation boundary point, and (4) supply diagnostic information on the execution and output the results for input to the flow solver. The reader are encouraged to find the details in [BSDB86, ST91] about PEGSUS.

2.1 Generation of Body-Fitted Grids

The chimera grid method makes use of body-fitted grids which we emphasize are an essential asset known to give viscous solutions accurately and economically, see for example [HC89, SIR94]. In the gridding process, the complete geometrical model is divided up into subdomains, which in general can be associated with components of a configuration. Each subdomain is gridded independently and is overset onto each other. The grid boundaries are not required to join in any special way. A number of grids can be introduced to focus on interesting geometrical or physical features. Figure 2 illustrates the chimera grid for the complex geometry of the integrated space shuttle vehicle, in which three grids conforming respectively the orbiter, external tank and solid rocket booster together with the associated hole boundaries are shown, representing a triumphant case for the method. A common or overlapped region is always required to provide the means of matching solutions

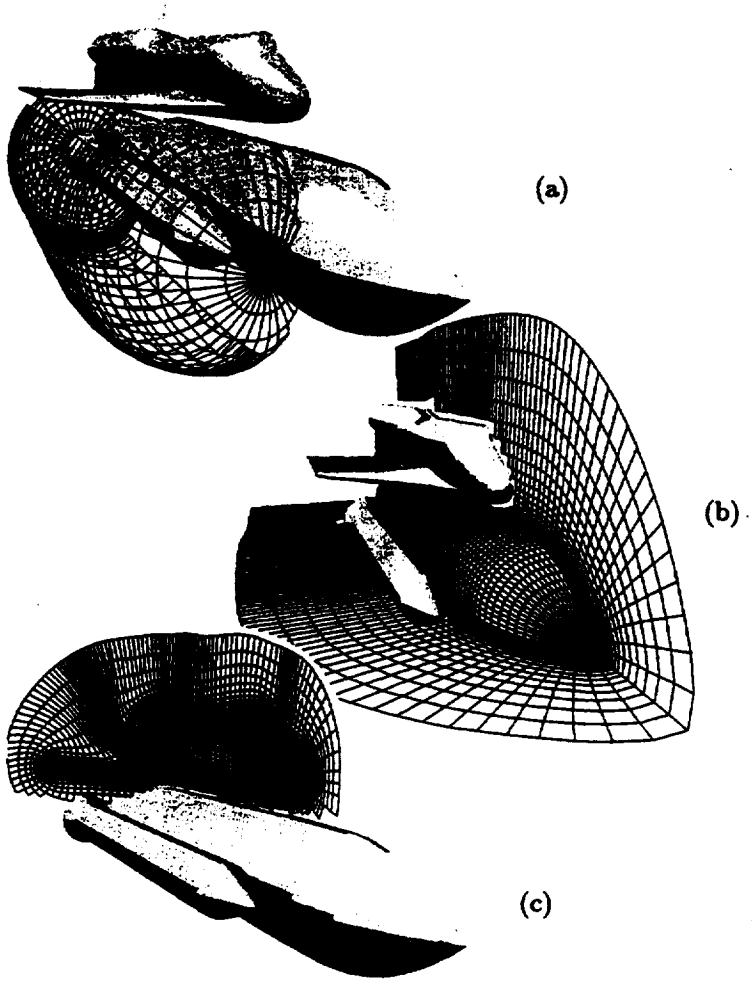

Figure 2 Chimera grid used for integrated space shuttle geometry consisting of orbiter, external tank (ET), and solid rocket booster (SRB) [MS89]: (a) SRB grid with ET and orbiter holes, (b) ET grid with SRB and orbiter holes, and (c) orbiter grid with ET and SRB holes.

across boundary interfaces.

2.2 Definition of Hole Boundary & Outer Boundary

Hole boundaries and outer boundaries are the two ways through which information is communicated from one grid to another. A novel approach used in the chimera method to distinguish a hole point and an outer boundary point from a field point is to flag the array IBLANK, which is dimensioned identically to the number of points in each grid, to either 1 for a field point or 0 otherwise. The boundary points with IBLANK=0 are to be updated by interpolation, while points with IBLANK=1 are updated as usual for the interior points.

2.2.1 Hole Boundary

Whenever points of a grid, say G_1, falls within the body boundary of another grid, say G_2, these points of G_1 are cut out to make a "hole" in G_1, as displayed earlier in Fig. 2. These hole points must also fall in the domain of G_2 to guarantee that a proper set of data from G_2 be communicated to G_1. Typically, a hole is defined through a hole creation boundary which consists of a surface or a group of surfaces. The purpose of a hole creation boundary is to identify points that are within this boundary. A grid point is considered to be inside a hole creation boundary if it is inside all surfaces that define the boundary.

Figure 3 illustrates how hole points are located using three surfaces, $S_1, S_2,$ andS_3, as the hole creation boundary. PEGSUS first puts the indices of all points of the grid in which the hole is to be created into a list. Then all points that fall outside surface S_1 are eliminated from the index list (as indicated by the shaded region). Then all points contained in the shortened list that are outside the surface S_2 are eliminated, resulting in an even shorter list. As the process is repeated for surface S_3, the points remaining in the list are the hole points of the grid in which the hole is created.

As noted earlier, the hole points are excluded from the solution (with IBLANK=0) and are not usable as boundary points for performing solution on the grid in which the hole is made. Therefore, grid points surrounding holes will be identified as fringe points which then constitute the hole boundary, see Fig. 4. To find hole boundary points, each point in the holed-grid is checked. If the point is a hole point, nothing is done. If the point is a field point and is next to a hole point, it is identified as a hole boundary point.

It must be noted that the PEGSUS code, even though very powerful and general, should not be taken as error-free. Some problems may arise, for example when the slope can not be uniquely defined either on a hole creation boundary or on the grid. Using the PEGSUS, as any other new techniques and softwares, will require some knowledge about the underlying techniques and experiences. Fortunately,

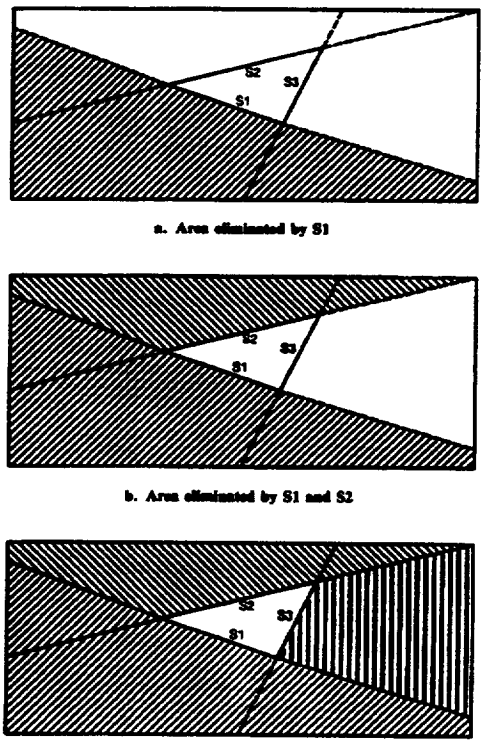

Figure 3 Hole creation by boundaries S_1, S_2, and S_3.

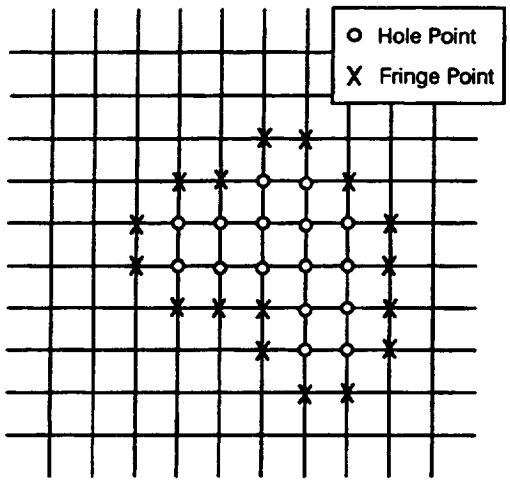

Figure 4 Hole boundary with single fringe points indicated by $\times$.

PEGSUS has enough flexibility and some ingenuity on the user's part can usually resolve difficulties.

2.2.2 Outer Boundary

The outer boundary on which the points are to be either interpolated or specified as physical boundary is directly input by giving the index range in each dimension. Then, the interpolation procedure is accomplished in almost exactly the same way as hole boundary interpolation.

We summarize the grid-related portion of the chimera method in Fig. 5 by displaying: (1) the overlapping of two grids, respectively designated as major and minor grids, with the latter being thought of conforming a component, (2) the hole creation boundary specified as a level surface in the minor grid and the fringe-point boundary in the major grid, and (3) the outer boundary in the minor grid.

2.3 Interpolation

Since the separate grids are to be solved independently, boundary conditions must be made available. Boundary conditions on the interpolated hole boundary and interpolated outer boundary are supplied from the grid in which the boundaries are contained. There are currently several approaches (e.g., [BSDB86, Ber84, BCH89, Rai86, ML89, WY94]) to obtain data for these conditions, but all involve some form of interpolation of data in a grid. Generally they can be grouped into two

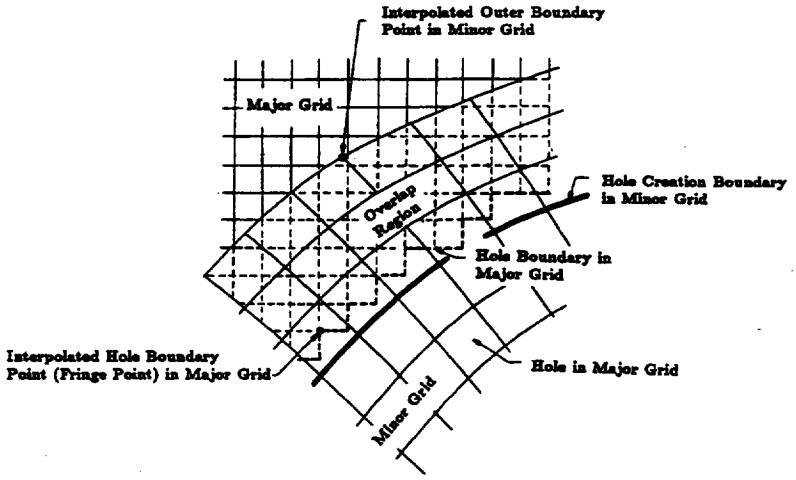

Figure 5 Construct of the chimera grid.

categories: nonconservative and conservative interpolations, which are discussed in the following.

2.3.1 Nonconservative Interpolation

Once the interpolation stencils are searched and identified, PEGSUS employs a nonconservative trilinear interpolation scheme, whose details are documented in [BSDB86]. There is much uncertainty as to measuring the local or global effects of the nonconservative interpolation on the solution, especially when a strong-gradient region intersects the interpolated region. Study on this subject has been scarce in the literature. Our experience (unpublished and published[KL94]) indicates that significant error can appear. For steady problems, a shock may be placed at incorrect location and noticeable spurious waves can eminate from the boundary of the interpolated region. For unsteady problems[KL94], the shock strength and speed is affected as the shock goes through the region of interpolation. In [CH90], the order of interpolation has been studied in relation to the order of the PDE, the order of the discretization, and the width of interpolation stencils for a model boundary value problem. For a second order differential equation discretized with a second order formula, it was found necessary to use an interpolant at least of third order, as the overlap width is on the order of the grid size. An assessment of their proposal's validity for a range of problems is warranted because interpolating has the advantage of being relatively simple matter to perform.

2.3.2 Conservative interpolation

It has been asserted that conservation property need be enforced for the cases in which shock waves or other high-gradient regions cross the region of interpolation. Several conservative interpolation schemes have been proposed for patched interfaces[Rai86, BO84] and arbitrarily overlapped regions[ML89]. These schemes are relatively easy in a 2D domain, but still substantially more complex than the nonconservative schemes. Their extensions to 3D are extremely difficult, if not impossible. Simplification is possible[KM91, TWR+89] for patched grids in 3D, but more restrictions on grid generation, making them less attractive, are placed.

A fundamental deficiency in all these approaches is that a choice has to be made concerning the distribution of fluxes from one grid to another, even though the sum of fluxes can be made conservative. Since the overlapped region is necessarily arbitrary, there will be great disparity in grid density and orientation along the overlapped region (or hole boundary). The choice of weighting formulas is not clear and certainly not unique.

3 DRAGON GRID

We conclude from the previous section that (1) maintaining grid flexibility and the quality of the chimera method are definitely to be preserved and even maximized (improved), but (2) focusing on improving (choosing) interpolation schemes perhaps only leads to more complication and does not seem to be a fruitful way to follow.

An alternative method which avoids interpolation altogether and strictly enforces flux conservation for both steady and unsteady problems is to solve the region in question on the same basis as the rest of the domain.

Since the overlapped region (thus, the hole boundary) is necessarily irregular in shape, the unstructured grid method is most suitable for gridding up this region. Furthermore, this region is in general away from the body where the viscous effect is less important compared to the inviscid effect, the unstructured grid would avoid penalty from accuracy consideration mentioned earlier. This combination of both types of grids results in a hybrid grid! In this approach we in effect Directly Replace Arbitrary Grid-Overlapping by a Non-structured grid. The resulting grid is thus termed the DRAGON grid. Major differences of our approach from other hybrid methods are:

- we heavily utilize the proven chimera method and the powerful and versatile automatic code PEGSUS, thus retaining attractive features listed previously in the **INTRODUCTION**,
- we use unstructured grids only in a limited region and located away from viscous-dominant regions, thus minimizing disadvantages of unstructured grids,

In addition, for discretizing the flux terms, we use the recently developed upwind scheme AUSM$^+$ [Lio94] which has been shown to be accurate, efficient, and reliable.

In what follows we will separately describe the structured and unstructured grid features of the DRAGON grid method.

3.1 Structured Grid Region

The PEGSUS code now is used and modified to provide information necessary for the DRAGON grid. The algorithmic steps are enumerated as follows.

1. As in the chimera grid, the entire computation domain is divided up into subdomains. We often designate a major grid enclosing the complete computational domain and the component grids as minor grid.
2. Hole regions are created, see Fig. 6(a), and the IBLANK array generated in which the elements associated with grid points inside the hole boundary are set to 0 (default value is 1). For example, the outer boundary of a minor grid is used as the hole creation boundary.
3. Both fringe points (hole boundary points) and interpolation boundary points are no longer treated as blanked points. Instead, they are now represented as interior points, and their IBLANK values are set to 1 (rather than 0) in the PEGSUS code. A file containing the coordinates of these points is obtained as output of the PEGSUS and these points will be used as boundaries for the unstructured grid region. Details for the unstructured grid will be addressed shortly.
4. Since interpolation process is no longer performed between structured grid blocks, output files providing interpolation information are deleted from the PEGSUS code.

It is noted that in step 2 we now have more freedom in defining the hole creation boundary for there is no need of requiring that grids overlap. When no overlapped region is found, then the empty space will be filled with an unstructured grid, thus resulting in a much more robust and flexible procedure.

This completes the portion of structured grid in the DRAGON grid.

3.2 Non-Structured Grid Region

The gap region created by arbitrarily overset grids inevitably is of irregular shape and would be very difficult to represent it with structured grids. Unstructured grids are most suitable to fill in this irregular-shaped space. Triangular cells, especially, can provide a good deal of flexibility to adapt to the odd shape. Recall, one important feature in the DRAGON grid is to eliminate any cumbersome interpolation. Unstructured grids alone are not sufficient to do the task. An additional constraint to the grid generation is imposed to require that the *boundary*

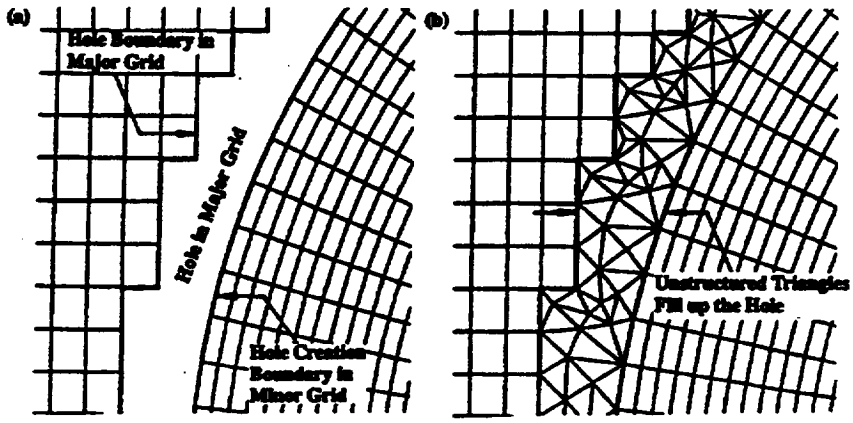

Figure 6 Direct Replacement of Arbitrary Grid-Overlapping by Non-structured gird: (a) chimera grid, (b) DRAGON grid.

nodes of the structured grid, which are output from the PEGSUS code, coincide with vertices of boundary triangular cells. Fortunately, this constraint fits well in unstructured grid generation. The Delaunay triangulation scheme[Bow81] is applied to generate an unstructured grid in the present paper. Figure 6(b) depicts the unstructured grid filling up the hole created in the structured grid by the chimera method. The steps adopting the unstructured cells in the framework of the chimera grid scheme are summarized below.

1. Boundary nodes provided by the PEGSUS code are reordered according to their geometric coordinates.
2. Delaunay triangulation method is then performed to connect these boundary nodes based on the Bowyer algorithm[Bow81].
3. In the unstructured grid, since there is no logical ordering of the cells and their neighbors, connectivity matrices containing the cell-based as well as edge-based information are introduced. Also the present approach requires additional matrices to connect the structured and unstructured grids. The connectivity matrices used in the present 2D version are summerized as follows.
   (a) IEDGENODE(1:2, edges) — 2 nodes for each edge,
   (b) ICELLEDGE(1:3, cells) — 3 edges for each triangular cell,
   (c) IEDGECELL(1:2, edges) — 2 neighboring cells for each edge,
   (d) IEDGETYPE(edges) — edge type (type of boundary condition),
   (e) IEDGEFLUX(grids, edges) — edge number that connects structured and unstructured grids, where the parameter "grids" identifies which structured

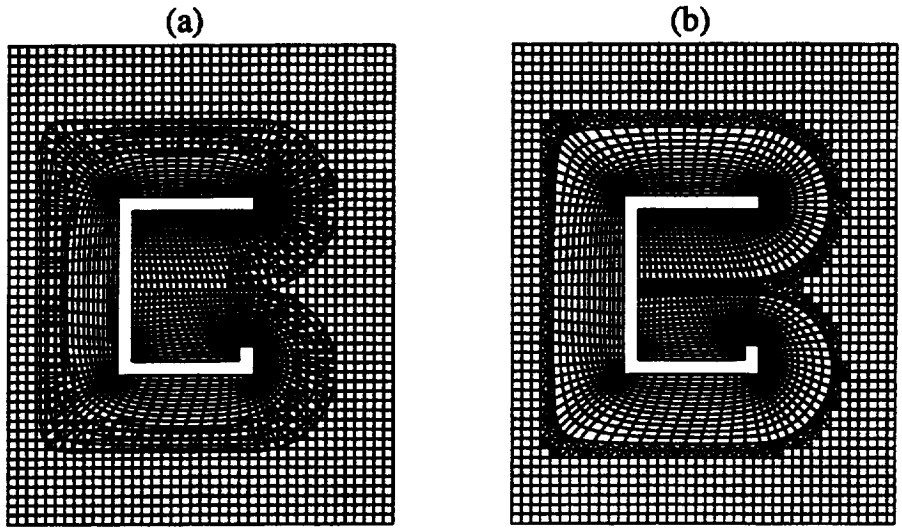

Figure 7 Comparison of the (a) chimera and (b) DRAGON grids for the letter "C" in a channel.

grid,

(f) IFLUXINDX(grids, edges) — i-index of the structured cell that shares the edge fluxes with the unstructured cell,

(g) IFLUXINDY(grids, edges) — j-index of the structured cell that shares the edge fluxes with the unstructured cell.

The first four types of connectivities are standard in unstructured grid codes, except that we assign "+" and "–" values to IEDGETYPE to indicate whether the outward normal vector of a triangulr cell face points into or out of the neighboring structured cell which shares the same face. This information is needed as the flux on this face, calculated based on the unstructured grid data, will be used also for the structured cell in order to exactly maintain consistency (conservation) of fluxes.

Questions concerning triangulr grid quality and improvements are not pursued for they are beyond the scope of the present paper.

This step completes the specification of the initial grid. Figure 7 now compares the DRAGON grid and the chimera grid for the letter "C" in a channel. The chimera method wraps around the "C" with a body-conforming (minor) grid and oversets it on the background (major) H-type grid. Note that we intentionally make an unsymmetric "C" to emphasize grid flexibility.

4 FLOW SOLVER

4.1 Governing Equations

The time-dependent compressible Euler equations, expressed in an integral form over an arbitrary control volume Ω are:

$$\int_{\Omega} \frac{\partial \mathbf{U}}{\partial t} dv + \int_{\partial\Omega} \vec{\mathbf{F}} \bullet d\vec{S} = 0,$$

where the conservative-variable vector $\mathbf{U} = (\rho, \rho u, \rho v, \rho w, \rho e_t)^T$. The inviscid flux is written as a sum of the convective and pressure fluxes: $\vec{\mathbf{F}} = \mathbf{\Phi}\vec{V} + \vec{\mathbf{P}}$, where $\mathbf{\Phi} = (\rho, \rho u, \rho v, \rho w, \rho h_t)^T$, is the vector containing convected variables and $\vec{\mathbf{P}} = p(0, \vec{i}, \vec{j}, \vec{k}, 0)^T$. The specific total energy is $e_t = e + |\vec{V}|^2/2 = h_t - p/\rho$. We denote with an overhead arrow the vector quantities expressed in terms of Cartesian coordinates.

4.2 Flux Splitting

Based on the cell-centered finite volume method, the governing equations are semi-discretized. We use the new flux scheme AUSM$^+$, described in full details in [Lio94], to express the numerical flux at the cell faces. The basic idea of AUSM$^+$ follows that of its predecessor, AUSM[LS93], but has substantial improvements. The AUSM$^+$, incurring negligible additional cost over AUSM per flux, allows an exact capture of a normal shock by using a suitably chosen interface speed of sound, yields smoother solution by way of including higher-order polynomials, and leads to faster convergence rate.

The semi-discretized form, describing the rate of time change of $\mathbf{U}$ in Ω via balance of fluxes through all enclosing faces, $\vec{S}_l, l = 1, \cdots, LX$, whether they be in the structured or unstructured grid regions, can be cast as

$$\int_{\Omega} \frac{\partial \mathbf{U}}{\partial t} dv + \sum_{l=1}^{LX} \vec{\mathbf{F}}_l \bullet \vec{S}_l = 0.$$

The last terms account for only normal components of the flux at the face, of which the equations are written in terms:

$$\int_{\Omega} \frac{\partial \mathbf{U}}{\partial t} dv + \sum_{l=1}^{LX} \mathbf{F}_{nl} |\vec{S}_l| = 0,$$

where $\mathbf{F}_{nl} = \vec{\mathbf{F}}_l \bullet \vec{n}_l$ and $\vec{n}_l$ is the unit normal vector of $\vec{S}_l$. The task is then to represent the numerical flux at the cell interface $\vec{S}_l$, which straddles cells denoted

by subscripts "L" and "R". The AUSM$^+$ scheme gives the numerical flux in the following expression.

$$\mathbf{F}_{nl} = \tilde{M}_l \frac{a_l}{2}(\mathbf{\Phi}_L + \mathbf{\Phi}_R) - |\tilde{M}_l| \frac{a_l}{2} \Delta\mathbf{\Phi} + \mathbf{P}_{nl}.$$

In this formula, a_l is the speed of sound suitably defined at the interface to result in an exact resolution of a normal shock[Lio94]. The interface Mach number M_l is an important variable and defined in the following steps.

1. Project velocity vectors at the cell centers, "L" and "R", to $\vec{S}_l$,

$$\tilde{V}_L = \vec{V}_L \bullet \vec{n}_l, \quad \tilde{V}_R = \vec{V}_R \bullet \vec{n}_l.$$

2. Define the corresponding Mach numbers,

$$\tilde{M}_L = \frac{\tilde{V}_L}{a_l}, \quad \tilde{M}_R = \frac{\tilde{V}_R}{a_l},$$

3. Define the interface convective Mach number by writing

$$\tilde{M}_l = \tilde{M}_L^+ + \tilde{M}_R^-,$$

where

$$\tilde{M}_L^+ = \begin{cases} \frac{1}{2}(\tilde{M}_L + |\tilde{M}_L|), & \text{if } |\tilde{M}_L| \geq 1, \\ M_\beta^+(\tilde{M}_L), & \text{otherwise,} \end{cases} \qquad \tilde{M}_R^- = \begin{cases} \frac{1}{2}(\tilde{M}_R - |\tilde{M}_R|), & \text{if } |\tilde{M}_R| \geq 1, \\ M_\beta^-(\tilde{M}_R), & \text{otherwise.} \end{cases}$$

The formulas for $M_\beta^\pm(M)$ are expressed in terms of eigenvalues of the nonlinear waves, $M+1$ and $M-1$[Lio94].

4. Define the interface pressure p_l in terms of the above-defined Mach numbers,

$$p_l = p_L^+(\tilde{M}_L) + p_R^-(\tilde{M}_R),$$

where p_L^+ and p_R^- are defined in a similar fashion as $\tilde{M}_L^+$ and $\tilde{M}_R^-$, and we get

$$\mathbf{P}_{nl} = p_l \begin{pmatrix} 0 \\ n_{l_x} \\ n_{l_y} \\ n_{l_z} \\ 0 \end{pmatrix}.$$

5. Assemble the interface numerical flux by upwind-selecting the convected variable $\mathbf{\Phi}$,

$$\mathbf{F}_{nl} = a_l(\tilde{M}_l^+ \mathbf{\Phi}_L + \tilde{M}_l^- \mathbf{\Phi}_R) + \mathbf{P}_{nl} = \tilde{M}_l \frac{a_l}{2}(\mathbf{\Phi}_L + \mathbf{\Phi}_R) - |\tilde{M}_l| \frac{a_l}{2} \Delta\mathbf{\Phi} + \mathbf{P}_{nl}.$$

4.3 Time Integration

The time integration scheme updates the conservative variables at the cell center. The present method originates from the Taylor series expansion in time, as was done in the Lax-Wendroff scheme. Then a two-step scheme, called predictor and corrector steps, with second order time accuracy can be obtained [LH89].

Predictor:

$$\mathbf{U}^* = \mathbf{U}^n + \Delta t \frac{\partial \mathbf{U}^n}{\partial t}$$

Corrector:

$$\mathbf{U}^{**} = \mathbf{U}^* + \Delta t \frac{\partial \mathbf{U}^*}{\partial t}$$

$$\mathbf{U}^{n+1} = \frac{1}{2}(\mathbf{U}^n + \mathbf{U}^{**}) = \frac{1}{2}\left\{\mathbf{U}^* + [\mathbf{U}^n + \Delta t \frac{\partial \mathbf{U}^*}{\partial t}]\right\}$$

It is noted that (1) the predictor step allows a full time step, and (2) like other 2-step integration schemes, only two levels of storage are needed as $\mathbf{U}^n$ is absorbed in forming the residual indicated in the squared bracket, (3) both predictor and corrector steps are identical, with no need of defining a midpoint for the corrector step, leading to simplification of coding and the complexity of evaluating the transport terms.

The stability of the scheme is restricted by the CFL (Courant-Friedrichs-Lewy) number not exceeding unity. For steady state cases, local time stepping is used to accelerate convergence.

As in the chimera method, each subdomain grid, including the unstructured grids, is solved independently, the inter-grid communication, which is vital for properly propagating flow variations throughout grids, must be established and is the subject of next section.

4.4 Data Communication Through Grid Interface

In the chimera method, this communication is made through the hole boundary or the outer boundary. Since the interface treatment methods are not necessarily satisfying any form of conservative constraints, the solutions on overlaid grids are often mismatched with each other. More seriously, this may ultimately lead to spurious or incorrect solutions, especially when a shock wave or high-gradient region passes through boundaries of overlaid grids, as will be seen later.

In the current work, both the structured and unstructured flow solvers were based on the cell center scheme in which the quadrilateral and triangulr cells are used respectively. Figure 8 shows the interfaces connecting both structured

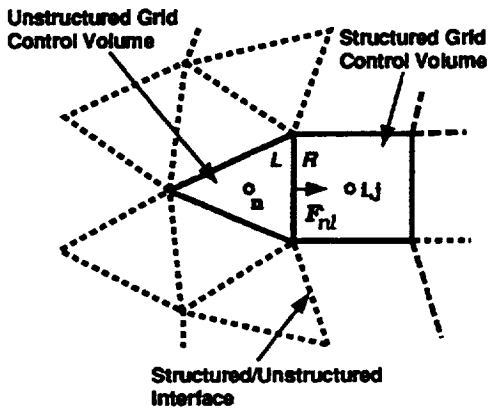

Figure 8 Fluxes at the cell face connecting the structured and unstructured grids.

and unstructured grids. As described earlier, the numerical fluxes, evaluated at the cell interface, are based on the conditions of neighboring cells ("L" and "R" cells). For the unstructured grid, the interface flux, $\mathbf{F}_{nl}$, will be evaluated using the structured-cell value as the right ("R") state and the unstructured-cell value as the left ("L") state. Consequently, the interface fluxes which have been evaluated in the unstructured process can now be directly applied in computing the cell volume residuals for the structured grid.

Thus, the communication in the DRAGON grid is considered seamless in the sense that no manipulation of data, which introduces uncertainties, is required, and the solution is obtained on the same basis whether it be in the structured or unstructured grid region. Consequently this strictly enforces conservation property locally and globally.

5 TEST CASES

Computational results are presented in this section for two-dimensional, inviscid problems. The test cases include a 2D shock tube problem and a supersonic flow past a letter "C" in a channel. Other results can be found in the report[KL94]. Since our unstructured flow solver is only first-order accurate, the same order of accuracy was also chosen for the structured solver. Implementation of higher-order accurate procedure to the unstructured code is currently underway. For the DRAGON grid approach, both structured and unstructured results can be displayed on the same plot using the Flow Analysis Software Toolkit (FAST) visualization package [WCM+93] on an IRIS workstation.

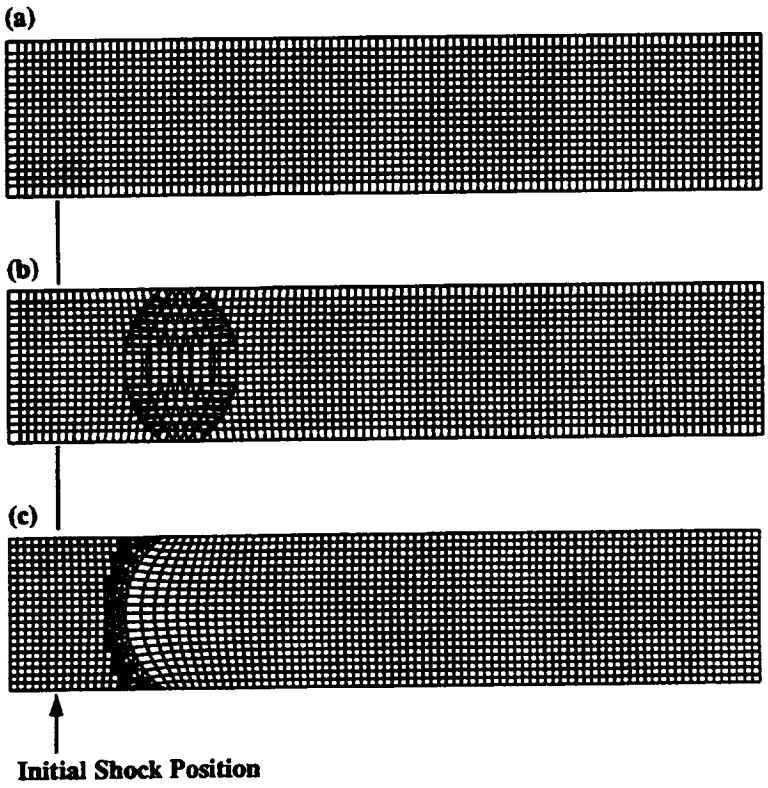

Figure 9 Grids for moving shock problem ($M_s = 4$): (a) single grid, (b) chimera grid, and (c) DRAGON grid.

Case 1: Shock Tube Problem

It has been of concern in CFD community that inaccurate shock speed and strength may result if the numerical procedure is not fully conserved. This case serves to show the effect of interpolation in the chimera grid and the validity of the DRAGON grid method for a transient problem as a plane shock moves across the embedded-grid region. The shock wave is moving into a quiescent region in a constant-area channel with a designed shock speed $M_s = 4$. Solutions were obtained using three grid systems, namely (1) single grid, (2) chimera grid, and (3) DRAGON grid, as displayed in Fig. 9. The single grid is dimensioned 801×21. The solution on this grid will be used for benchmark comparison. Figure 9(b) illustrates the chimera grid which includes a major grid (upstream region) of size 41×21, and a minor grid (downstream region) of dimension 781×21. The grid lines in the overlaid grids are generated in any arbitrary fashion. Upon the replacement of

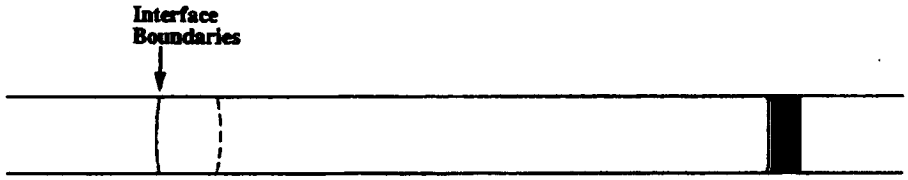

Figure 10 Pressure contours of the moving shock problem.

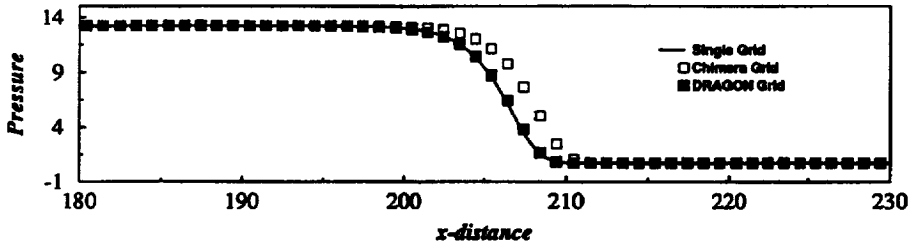

Figure 11 Comparison of centerline pressures from the three grids.

grid-overlapping by non-structured grid, the DRAGON grid is shown in Fig. 9(c). Note that all three grid systems use equivalent grid densities in major portion of the computation domain, except for that near the interface boundaries.

The initial conditions to the left and right of the shock (marked in Fig. 9) are:

$$\begin{pmatrix} \rho \\ p \\ u \\ v \end{pmatrix}_L = \begin{pmatrix} 4.57 \\ 13.21 \\ 3.125 \\ 0 \end{pmatrix}, \quad \begin{pmatrix} \rho \\ p \\ u \\ v \end{pmatrix}_R = \begin{pmatrix} 1 \\ 0.71 \\ 0 \\ 0 \end{pmatrix}.$$

Figure 10 displays the pressure contours after 500 time steps; all three grids give similar clean contours after the shock wave has passed through the interface boundaries. However, a critical comparison of the pressure distributions along the centerline of the channel, as plotted in Fig. 11, shows that the chimera scheme predicts a faster moving shock in the tube, while the present DRAGON grid and the single grid results coincide, indicating that the shock is accurately captured and conservation property well preserved when going through the region of the embedded DRAGON grid.

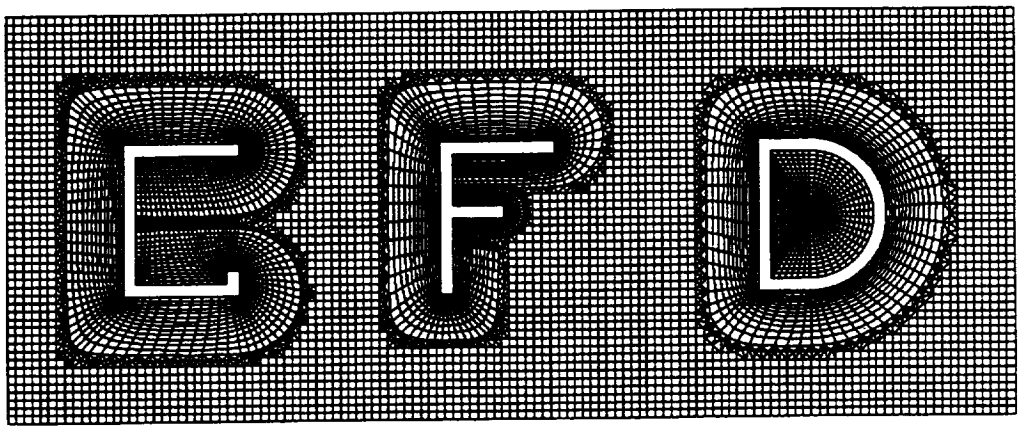

Figure 12 DRAGON grid for letters "CFD".

Case 2: Supersonic Shock Passing "C"-Body

This case is intended to show (1) the effectiveness of the DRAGON method for handling complex geometries involving odd shapes and composites of different grid topologies, and (2) the performance of the solution near the hybrid grid region. Figure 12 shows the DRAGON grid generated for the letters "CFD" according to the procedure outlined in this paper. In this example, we have hybridizations of "C-H" grids for letters "C" and "F" and "O-H" grids for "D". In "F", there is also a hybridization of "C-C" grids. The strength of the chimera and thus the DRAGON methods is exemplified here since (1) each letter is wrapped (easily) with a body-conforming grid which also well resolves sharp corners, and (2) each letter-grid is generated independently and can be moved about at will without affecting other grids. Furthermore, it can be imagined readily (although not demonstrated here) that grid enrichment for resolving geometry or flow details can be added on in a specified region, or vice versa for the reverse process.

Next we show the time evolution of flow as a supersonic shock starts moving toward the "C"-body. Figure 13 displays pressure-contours snap shots of the flow at three representative times. It should be noted that the contour lines smoothly cross the intersection boundaries of the structured and unstructured cells. Figure 14 displays the close-up view of the flow near the corners in "C" at the last instant. Note in both figures that small gaps interrupting the contour lines are observed along the interface boundaries because cell center values are displayed in the structured grid region while in the unstructured grid region variables are ploted at cell vertices.

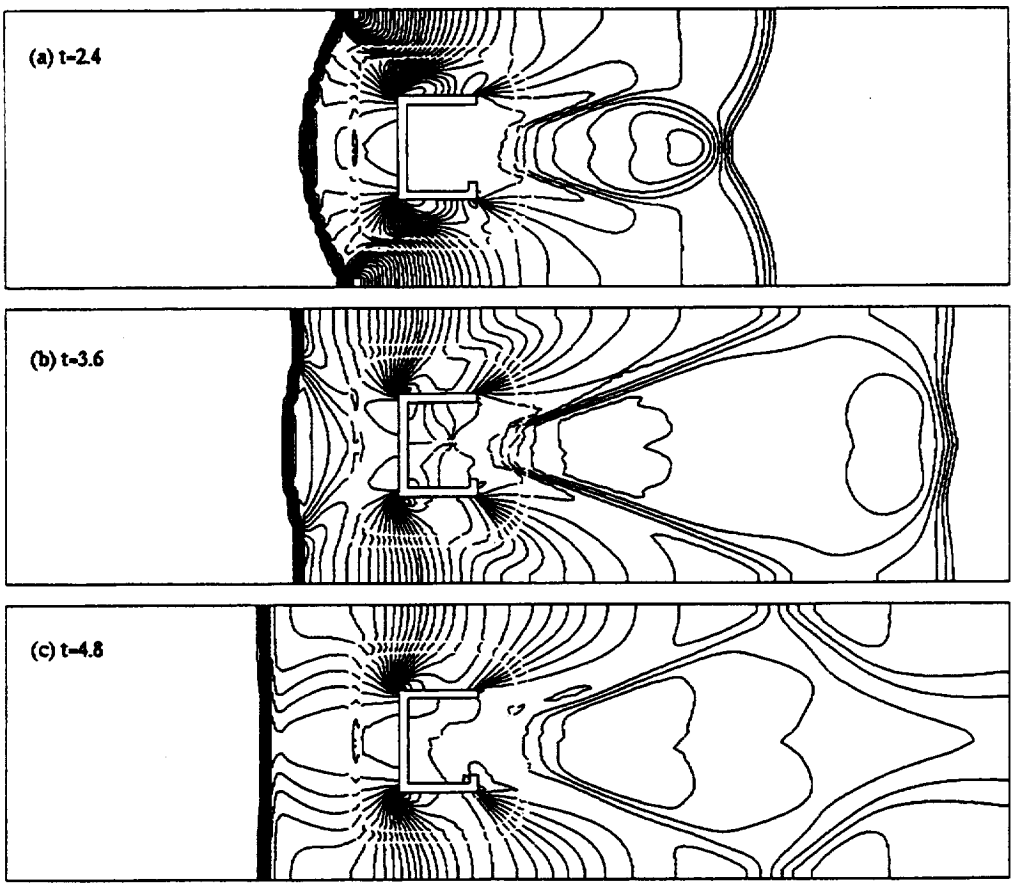

Figure 13 Evolution of flow, as depicted by pressure contours, about the "C" at three representative times.

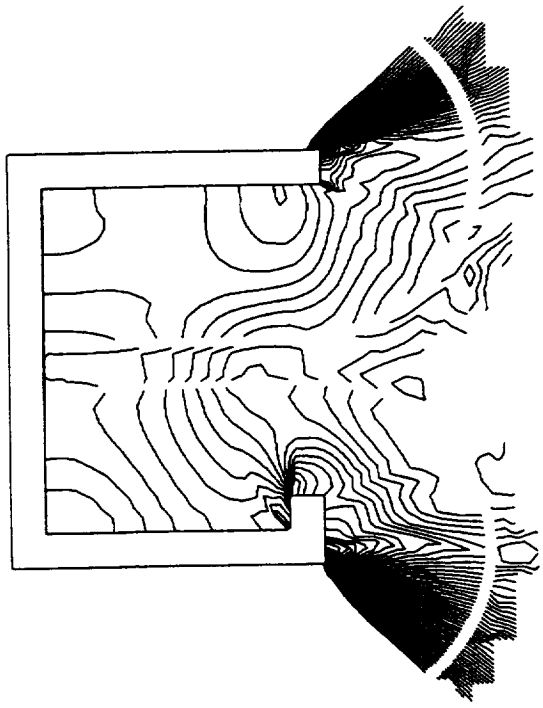

Figure 14 Close-up view of pressure contours about the "C" at $t = 4.8$.

6 CONCLUSION

In this paper we presented a new approach, termed the DRAGON grid, that uses non-structured meshes to replace the arbitrarily overlapped structured regions in the framework of the chimera grid. It is designed to further enhance the flexibility of the chimera embedded-grids technique and to enforce conservative grid communication between embedded grids. Numerical results have born out the validity of the DRAGON method. Currently we are focusing on enhancements for unstructured grid solver and generation in 3D; results will be reported soon.

Acknownledgements

We would like to thank Drs. P. Jorgenson and James Loellbach for their help in generating the unstructured grids and providing the basic code of an unstructured flow solver.

REFERENCES

[Att81] Atta E. H. (1981) Component-adaptive grid interfacing. AIAA Paper 81-0382, AIAA 19th Aerospace Sciences Meeting, St. Louis, MO.

[BCH89] Brown D. L., Chesshire G., and Henshaw W. D. (1989) Getting started with CMPGRD, introductory user's guide and reference manual. LA-UR-89-1294, Los Alamos National Laboratory.

[BCM+89] Buning P. G., Chiu I. T., Martin F. W., L.Meakin R., Obayashi S., Rizk Y. M., Steger J. L., and Yarrow M. (1989) Flowfield simulation of the space shuttle vehicle in ascent. In *Proc. Fourth International Conference on Supercomputing.* Santa Clara, CA.

[Ber84] Berger M. J. (1984) On conservation at grid interfaces. ICASE Report 84-43, NASA Langley Research Center, Hampton, VA.

[BO84] Berger M. J. and Oliger J. (1984) Adaptive mesh refinements for hyperbolic partial differential equations. *J. Comput. Phys.* 53: 484.

[Bow81] Bowyer A. (1981) Computing Dirichlet tessellations. *The Computing J.* 24: 162.

[BS93] Blake K. R. and Spragle G. S. (1993) Unstructured 3d Delaunay mesh generation applied to planes, trains and automobiles. AIAA Paper 93-0673, AIAA 31th Aerospace Sciences Meeting & Exhibit, Reno, NV.

[BSDB86] Benek J. A., Steger J. L., Dougherty F. C., and Buning P. G. (1986) *Chimera: A Grid-Embedding Technique, AEDC-TR-85-64.* AEDC.

[CH90] Chesshire G. and Henshaw W. D. (1990) Composite overlapping meshes for the solution of partial diffential equations. *J. Comput. Phys.* 90: 1.

[Gha94] Ghaffari F. (1994) On the vortical-flow prediction capability of an unstructured-grid Euler solver. AIAA Paper 94-0061, AIAA 32nd Aerospace Sciences Meeting & Exhibit, Reno, NV.

[HC89] Holmes D. G. and Connell S. D. (1989) Solution of the 2d Navier-Stokes equations on unstructured adaptive grids. AIAA Paper 89-1932, AIAA 9th CFD Conference, Buffalo, NY.

[JBW86] Jameson A., Baker T. J., and Weatherill N. P. (1986) Calculation of inviscid transonic flow over a complete aircraft. AIAA Paper 86-0103, AIAA 24th Aerospace Sciences Meeting, Reno, NV.

[KL94] Kao K.-H. and Liou M.-S. (1994) Direct replacement of arbitrary grid-overlapping by non-structured grid. NASA TM 106601, Lewis Research Center, Cleveland, Ohio.

[KLC94] Kao K.-H., Liou M.-S., and Chow C. Y. (1994) Grid adaptation using chimera composite overlapping meshes. *AIAA J.* 32: 942.

[KM91] Klopfer G. H. and Molvik G. A. (1991) Conservative multi-zonal interface algorithm for the 3d Navier-Stokes equations. AIAA Paper 91-1601-CP, AIAA 10th CFD Conference, Honolulu, Hawaii.

[LH89] Liou M.-S. and Hsu A. T. (1989) A time accurate finite volume high resolution scheme for three dimensional Navier-Stokes equations. AIAA Paper 89-1994-CP, AIAA 9th CFD Conference, Buffalo, NY.

[Lio94] Liou M.-S. (1994) A continuing search for a near-perfect numerical flux scheme, Part I: AUSM+. NASA TM 106524, Lewis Research Center, Cleveland, Ohio. Also submitted for journal publication.

[Löh87] Löhner R. (1987) An adaptive finite element scheme for transient problems in cfd. *Computer Methods in Applied Mechanics and Engineering* 61: 323.

[LS93] Liou M.-S. and Steffen C. J. (1993) A new flux splitting scheme. *J. Comput. Phys.* 107: 23.

[ML89] Moon Y. J. and Liou M.-S. (1989) Conservative treatment of boundary interfaces for overlaid grids and multi-level grid adaptations. AIAA Paper 89-1980-CP, AIAA 9th CFD Conference, Buffalo, NY.

[MS89] Meakin R. L. and Suhs N. (1989) Unsteady aerodynamic simulation of multiple bodies in relative motion. AIAA Paper 89-1996-CP, AIAA 9th CFD Conference, Buffalo, NY.

[NO87] Nakahashi K. and Obayashi S. (1987) Fdm-fem zonal approach for viscous flow computations over multiple-bodies. AIAA Paper 87-0604, AIAA 25th Aerospace Sciences Meeting, Reno, NV.

[Pro93] Proceedings (1993) In Posenau M. (ed) *Unstructured Grid Generation Techniques and Software, NASA CP-10119.*

[PVMZ87] Peraire J., Vahdati M., Morgan K., and Zienkiewicz O. C. (1987) Adaptive remeshing for compressible flow computations. *J. Comput. Phys.* 72: 449.

[Rai86] Rai M. M. (1986) A conservative treatment of zonal boundaries for Euler equation calculations. *J. Comput. Phys.* 62: 472.

[SB87] Steger J. L. and Benek J. A. (1987) On the use of composite grid schemes in computational aerodynamics. *Comp. Methods Appl. Mech. and Eng.* 64: 301.

[SIR94] Soetrisno M., Imlay S. T., and Roberts D. W. (1994) A zonal implicit procedure for hybrid structured-unstructured grids. AIAA Paper 94-0645, AIAA 32nd Aerospace Sciences Meeting & Exhibit, Reno, NV.

[ST91] Suhs N. E. and Tramel R. W. (1991) *PEGSUS 4.0 User's Manual, AEDC-TR-91-8.* Calspan Corporation/AEDC Operations.

[Ste90] Steger J. L. (1990) Thoughts on the chimera method of simulation of three-dimensional viscous flow. In Liou M.-S. and Povinelli L. A. (eds) *Proc. Computational Fluid dynamics Symposium on Aeropropulsion, NASA CP-3078,* pages 1–10.

[TWR+89] Thomas J. L., Walters R. W., Reu T., Ghaffari F., Weston R., and Luckring J. M. (1989) Patched-grid algorithm for complex configurations directed towards the F/A-18 aircraft. AIAA Paper 89-0121, AIAA 27th Aerospace Sciences Meeting, Reno, NV.

[WCM+93] Walatka P. P., Clucas J., McCabe R. K., Plessel T., and Potter R. (1993) *FAST User Guide, RND-93-010.* NASA Ames Research Center.

[Wea88] Weatherill N. P. (1988) On the combination of structured-unstructured meshes. In Sengupta S., Häuser J., Eiseman P. R., and Thompson J. F. (eds) *Numerical Grid Generation in Computational Fluid Mechanics,* pages 729–739. Pineridge Press, Swansea, UK.

[WY94] Wang Z. J. and Yang H. Q. (1994) A unified conservative zonal interface treatment for arbitrarily patched and overlapped grids. AIAA Paper 94-0320, AIAA 32nd Aerospace Sciences Meeting & Exhibit, Reno, NV.

REPORT DOCUMENTATION PAGE

Form Approved
OMB No. 0704-0188

1. AGENCY USE ONLY (*Leave blank*)	2. REPORT DATE	3. REPORT TYPE AND DATES COVERED
	August 1994	Technical Memorandum

4. TITLE AND SUBTITLE

Progress in Grid Generation: From Chimera to DRAGON Grids

5. FUNDING NUMBERS

WU-505-62-52

6. AUTHOR(S)

Meng-Sing Liou and Kai-Hsiung Kao

7. PERFORMING ORGANIZATION NAME(S) AND ADDRESS(ES)

National Aeronautics and Space Administration
Lewis Research Center
Cleveland, Ohio 44135-3191

8. PERFORMING ORGANIZATION REPORT NUMBER

E-9071

9. SPONSORING/MONITORING AGENCY NAME(S) AND ADDRESS(ES)

National Aeronautics and Space Administration
Washington, D.C. 20546-0001

10. SPONSORING/MONITORING AGENCY REPORT NUMBER

NASA TM-106709
ICOMP-94-19

11. SUPPLEMENTARY NOTES

Meng-Sing Liou, NASA Lewis Research Center, and Kai-Hsiung Kao, Institute for Computational Mechanics in Propulsion, NASA Lewis Research Center (work funded under NASA Cooperative Agreement NCC3-233). ICOMP Program Director, Louis A. Povinelli, organization code 2600, (216) 433-5818.

12a. DISTRIBUTION/AVAILABILITY STATEMENT

Unclassified - Unlimited
Subject Category 02

12b. DISTRIBUTION CODE

13. ABSTRACT (***Maximum 200 words***)

Hybrid grids, composed of structured and unstructured grids, combines best features of both. The chimera method is a major stepstone toward a hybrid grid from which the present approach is evolved. The chimera grid composes a set of overlapped structured grids which are independently generated and body-fitted, yielding a high quality grid readily accessible for efficient solution schemes. The chimera method has been shown to be efficient to generate a grid about complex geometries and has been demonstrated to deliver accurate aerodynamic prediction of complex flows. While its geometrical flexibility is attractive, interpolation of data in the overlapped regions--which in today's practice in 3D is done in a nonconservative fashion, is not. In the present paper we propose a hybrid grid scheme that maximizes the advantages of the chimera scheme and adapts the strengths of the unstructured grid while at the same time keeps its weaknesses minimal. Like the chimera method, we first divide up the physical domain by a set of structured body-fitted grids which are separately generated and overlaid throughout a complex configuration. To eliminate any pure data manipulation which does not necessarily follow governing equations, we use non-structured grids only to directly replace the region of the arbitrarily overlapped grids. This new adaptation to the chimera thinking is coined the DRAGON grid. The nonstructured grid region sandwiched between the structured grids is limited in size, resulting in only a small increase in memory and computational effort. The DRAGON method has three important advantages: (1) preserving strengths of the chimera grid, (2) eliminating difficulties sometimes encountered in the chimera scheme, such as the orphan points and bad quality of interpolation stencils, and (3) making grid communication in a fully conservative and consistent manner insofar as the governing equations are concerned. To demonstrate its use, the governing equations are discretized using the newly proposed flux scheme, AUSM$^+$, which will be briefly described herein. Numerical tests on representative 2D inviscid flows are given for demonstration. Finally, extension to 3D is underway, only paced by the availability of 3D unstructured grid generator.

14. SUBJECT TERMS	15. NUMBER OF PAGES
Chimera grid; Unstructured grid; Hybrid grid; Upwind splitting	28
	16. PRICE CODE: A03

17. SECURITY CLASSIFICATION OF REPORT	18. SECURITY CLASSIFICATION OF THIS PAGE	19. SECURITY CLASSIFICATION OF ABSTRACT	20. LIMITATION OF ABSTRACT
Unclassified	Unclassified	Unclassified	